scientific reports

Check for updates

OPEN

Global optimization of an encapsulated Si/SiO_2 L3 cavity with a 43 million quality factor

J. P. Vasco✉ & V. Savona

We optimize a silica-encapsulated silicon L3 photonic crystal cavity for ultra-high quality factor by means of a global optimization strategy, where the closest holes surrounding the cavity are varied to minimize out-of-plane losses. We find an optimal value of $Q_c = 4.33 \times 10^7$, which is predicted to be in the 2 million regime in presence of structural imperfections compatible with state-of-the-art silicon fabrication tolerances.

Photonic crystal (PC) slab cavities have been focus of intense research during the last two decades due to their unique properties to efficiently confine light at length scales close to the diffraction limit, and extremely low loss rates[1,2]. These features have allowed to study a wide variety of classical and quantum phenomena, where the linear and non-linear interactions between light and matter are effectively enhanced in the cavity region[3–20]. Broadly speaking, the strength of this enhancement grows with the local density of electromagnetic states, which is proportional to the quality factor of the cavity mode Q_c, and inversely proportional to its mode volume V[21–23]. Hence, massive efforts have been directed toward the optimization of these figures of merit in order to reach the desired functionality of the photonic device[24–29]. Particularly, silicon-based cavities have attracted very much attention because of their natural compatibility with CMOS technologies and negligible material losses at telecom wavelengths, allowing the integration with optoelectronic devices in a single chip[30]. While free-standing silicon PC slabs offer an excellent platform to build ultralow loss cavities[27,31,32], silica (SiO_2) encapsulation improves the mechanical stability and thermal dissipation of the system[33], while mitigating additional loss channels coming from the etching of air holes in the silicon[34]. Nevertheless, high quality factors are challenging in such encapsulated structures given the low refractive index contrast between the two materials.

In this work, we employ a global optimization approach to maximize the quality factor of a Si/SiO_2 L3 PC cavity. Since it was proposed for first time by Y. Akahane et al.[2], the L3 cavity stands out as the paradigm of high-Q cavity with very small spatial footprint and small mode volume close to diffraction limit[24,35]. The resonant mode of the L3 cavity has Bloch components mostly lying below the radiative light cone, similarly to many other geometries of PC cavities. This configuration is well suited for optimization of the quality factor, as the small Bloch components still above the light cone—responsible for radiative losses—can be suppressed by small geometric tweaks of the cavity surroundings. For this reason, the L3 cavity has been the model of many recent optimization strategies, both with conventional Maxwell simulators and more recently with the help of deep learning[36]. Here, we find an optimal quality factor of $Q_c = 4.33 \times 10^7$, which corresponds to a remarkable low out-of-plane losses given the short length of the cavity. Our results set a new record for the L3 paradigm and open the way to a new class of highly efficient and ultra-compact optical devices for linear and non-linear applications in classical and quantum photonics.

L3 cavity optimization

We consider a silica-encapsulated silicon PC slab with a hexagonal lattice of holes of radii $r = 100$ nm, lattice parameter $a = 390$ nm and thickness $d = 220$ nm. Refractive indices of SiO_2 and Si are taken at telecom wavelengths, i.e., $n_{SiO_2} = 1.44$ and $n_{Si} = 3.47$, respectively. A L3 cavity is introduced by removing three holes along the ΓK direction of the lattice. In order to optimize the quality factor Q_c of its fundamental mode, we adopt a global optimization approach in which only the closest holes surrounding the cavity are varied, in size $r \to r + dr$ and position $(x, y) \to (x + dx, y + dy)$, to reduce out-of-plane losses. This technique has been extremely successful during the last few years to reach record theoretical and experimental quality factors for a wide variety

Institute of Physics, École Polytechnique Fédérale de Lausanne (EPFL), CH-1015 Lausanne, Switzerland. ✉email: juan.vasco@epfl.ch

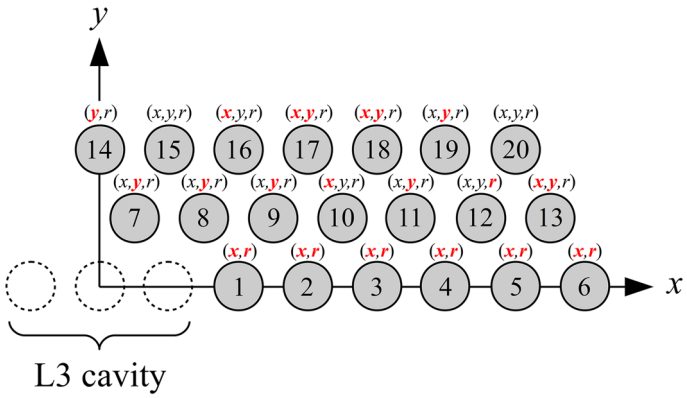

Figure 1. Schematic representation of the closest holes surrounding the L3 cavity, in the first quadrant, which are considered in the global optimization procedure. Mirror symmetry with respect to $x = 0$ and $y = 0$ is assumed, thus setting a total of 53 optimization parameters. Nevertheless, only the ones highlighted in red are found to be the most relevant to increase the fundamental mode quality factor.

Si/SiO_2 – L3 cavity	f (Thz)	Q_c	$V_l(\lambda/n_{Si})^3$	$V_{nl}(\lambda/n_{SI})^3$	$Q_c/N_l(n_{SI}/\lambda)^3$	$Q_c^2/V_{nl}^2(n_{SI}/\lambda)^6$
Non-optimized	195.2	1.33×10^3	0.67	3.25	1.99×10^3	1.68×10^5
Optimized	191.2	4.33×10^7	1.75	7.47	2.47×10^7	3.36×10^{13}

Table 1. Summary of the main linear and non-linear figures of merit of the non-optimized and optimized Si/SiO_2 L3 cavities.

of different materials and cavity geometries[20,25,27,35,37–39]. For a single optimization step, the quality factor of a given configuration must be efficiently computed. To this purpose, we use the guided mode expansion (GME) method[40] which, for PC slab structures, has proven to be as predictive as first-principle commercial Maxwell simulators like FDTD, while being several orders of magnitude faster (see methods). This allows to simulate hundreds of thousands configurations as needed by most optimization algorithms. In addition to a Maxwell solver, one needs an efficient global optimization algorithm to find the global maximum of the quality factor in the complex landscape in parameter space. For this, non-gradient-based algorithms have empirically proven to be very effective in the past. One in particular – the particle swarm (PS) algorithm – was successfully used in past PC optimization works and turned out to be very effective also in the present analysis. As an additional advantage, as discussed in what follows, the PS algorithm is embarrassingly parallel and can be run on a multi-core architecture with dramatic computational advantage. We show in Fig. 1 the schematic representation of the holes to be considered in the optimization procedure, where mirror symmetry with respect to the planes $x = 0$ and $y = 0$ is assumed. Thereby, we end up with a total of 53 optimization parameters. However, after 1400 iterations of the PS algorithm we have noted that the most relevant parameters for increasing Q_c are those highlighted in red in Fig. 1. This preliminary analysis allowed us to reduce the dimension of the optimization parameter space from 53 to 27, and decrease the number of function evaluations required by the algorithm to converge. We summarize in Table 1 our final results where

$$V_l = \frac{\int \epsilon(\mathbf{r})|\mathbf{E}(\mathbf{r})|^2 d\mathbf{r}}{\text{Max}\left\{\epsilon(\mathbf{r})|\mathbf{E}(\mathbf{r})|^2\right\}}, \tag{1}$$

is the linear mode volume and

$$V_{nl} = \frac{\left[\int \epsilon(\mathbf{r})|\mathbf{E}(\mathbf{r})|^2 d\mathbf{r}\right]^2}{\int \epsilon^2(\mathbf{r})|\mathbf{E}(\mathbf{r})|^4 d\mathbf{r}}, \tag{2}$$

is the non-linear one[41], with $\epsilon(\mathbf{r})$ representing the dielectric function of the system and $\mathbf{E}(\mathbf{r})$ the electric field of the cavity mode. An optimal solution of $Q_c = 4.33 \times 10^7$ (computed with FDTD[42]) is found after 806200 function evaluations, leading to an improvement of four orders of magnitude with respect to the non-optimized cavity. While this theoretical quality factor is around 50% of the record value achieved in glass-clad hetero-structured cavities[43], it corresponds to the largest reported for the encapsulated L3 cavity. Moreover, the short-length mode confinement provided by the L3 geometry is more convenient for applications in ultra-compact devices. It is noteworthy that, Q_c is maximized at the expense of the linear and non-linear mode volumes, in contrast to previous optimizations of the L3 cavity[25]. Nevertheless, we still get extremely large enhancement factors Q_c/V_l and Q_c^2/V_{nl}^2 which are in the 10^7 and 10^{13} regimes, respectively. The increase of the mode volume is clearly seen in the Fig. 2, where we plot the near-field intensity distribution of the fundamental cavity mode in the middle of

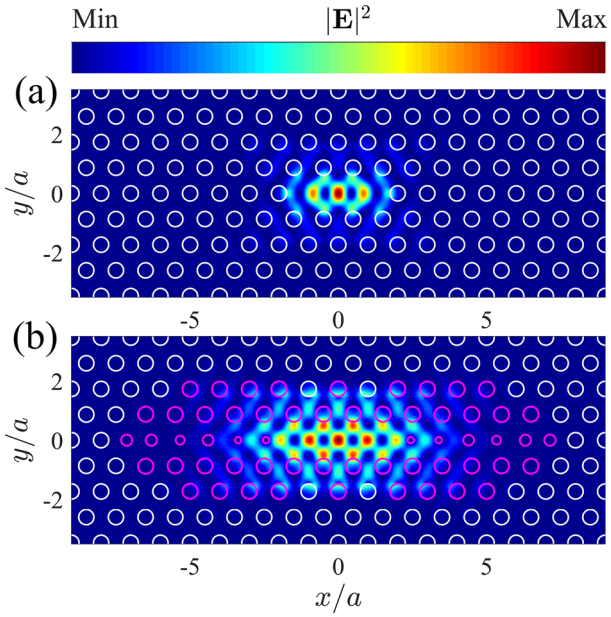

Figure 2. (**a**) Near-field intensity distribution of the non-optimized L3 fundamental mode cavity. (**b**) same as (a) for the optimized L3 cavity, where the holes which are actually considered in the optimization are represented by magenta circles.

the slab, for the non-optimized cavity, Fig. 2(a), and the optimized one, Fig. 2(b). The holes which are actually varied are represented by magenta circles in Fig. 2(b). The optimal parameters of the cavity as well as the far-filed projection of the near-field components are reported in the Supplementary Information.

The same optimization strategy can be directly applied to the air-bridge silicon L3 cavity within the same parameter space of dimension 27. For this configuration, we have obtained an FDTD quality factor $Q_c = 1.91 \times 10^8$. Such Q_c is around 20 times larger than the previous record obtained with deep neural networks[36], where a different set of parameters were considered to optimize the objective function. While our optimization requires a much larger number of evaluations to find the maximum of the objective function, it clearly shows that there is still considerable room for further improvement of these figures of merit by better identifying the optimization parameters. Detailed results for the Si/Air L3 cavity are given in the Supplementary Information.

Disorder analysis

Realistic photonic devices are always subject to a small amount of intrinsic disorder, coming from unavoidable imperfections introduced at the fabrication stage. We model such effect by considering random Gaussian fluctuations in all hole positions and radii of our PC, where the standard deviation of the Gaussian probability distribution σ is taken as the disorder parameter[44–46]. Results of this analysis are shown in Fig. 3, where the averaged cavity quality factor $\langle Q_c \rangle$, computed over 100 independent disorder realization of the system, is plotted as a function of σ. Typical tolerances in silicon state-of-the-art fabrication techniques range between $\sigma = 0.001a$ and $\sigma = 0.002a$[31,47], which leads to an averaged Q_c in the 2 million regime. Previous measured Q values on 2D PC slab cavities with low index claddings range from 0.6×10^6 (silica cladding)[48] to 1×10^6 (glass cladding)[43], with estimated disorder magnitudes larger than $\sigma = 0.002a$. However, the confinement mechanism is based on hetero-structured PCs waveguides or effective photonic potentials which usually require a long-length cavity region, i.e., more than 20 periods of the underlying photonic lattice.

Conclusions

In conclusion, we have optimized a silica-encapsulated silicon L3 cavity by means of a global optimization strategy, where the closest holes surrounding the cavity are varied to decrease out-of-plane losses. We have found a value of $Q_c = 4.33 \times 10^7$, corresponding to outstanding result given the short-length of the confinement region. To better relate our optimal design to realistic samples, we have also studied the effects of intrinsic disorder. When considering typical tolerances in modern fabrication techniques, the averaged quality factor of the optimized cavity remains in the 2 million regime, which is comparable to previous measurements in fully embedded hetero-structured and photonic potential based designs. Apart from setting a new record for the encapsulated L3 cavity, our results open the way to a new class of optimized designs in low-index-contrast materials, such as AlN, GaN or Si_3N_4, holding great promise for nonlinear optical enhancement, sensing, and solid-state quantum optics.

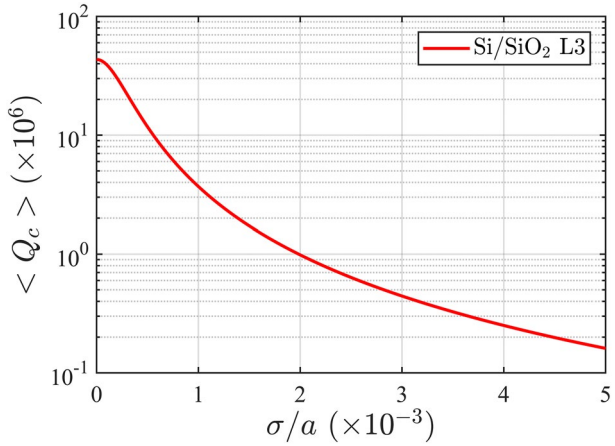

Figure 3. Averaged Q_c, computed over 100 independent disorder realizations of the optimal cavity, as a function of the disorder parameter σ.

Methods

The guided mode expansion. We employ the guided mode expansion method (GME)[40] as our main PC solver for estimating the cavity mode frequencies and quality factors at the optimization stage. The expansion was carried out in a supercell of dimensions $20a \times 7\sqrt{3}a$ with 8517 plane waves and one TE guided mode. During the optimization procedure we mainly focus on the growing direction of Q_c within the high-dimensional space of parameters. Therefore, only one k point is needed (in the Brillouin zone of the supercell) to compute the real $\Re\{\omega_c\}$ and imaginary $\Im\{\omega_c\}$ parts of the mode frequencies ω_c. The cavity quality factor, associated to out-of-plane losses, is thus defined as[40]

$$Q_c = \frac{\Re\{\omega_c\}}{2\Im\{\omega_c\}}. \tag{3}$$

Note that, while a single k point describes the topology of the optimization space with accuracy (which is enough for the PS algorithm), it does not give the actual value of Q_c. This is why the GME estimation of Q_c with a single k may differ significantly from the value computed with FDTD (see Supplementary information). In order to recover the absolute quality factor of the cavity with GME, Eq. (3) must be integrated over k in the Brillouin zone of the supercell.

Particles Swarm algorithm. We have used the parallel version of the Particles Swarm (PS) algorithm available in the Global Optimization Toolbox of MATLAB. It starts from a random swarm, uniformly distributed, of 139 particles and requires 5800 iterations to converge. Every particle at each iteration corresponds to an independent evaluation of Q_c with GME executed by one CPU core. The total number of cores used in the computation is 139. This results in 806200 GME simulations to find the maximum of the objective function Q_c. It is worth mentioning that the number of iterations can be reduced by increasing the number of particles in the swarm, which may be advantageous if more cores are employed in the optimization.

FDTD numerical experiments. Once the optimal parameters are found by the PS optimization, we simulate the final structure with a commercial FDTD solver[42]. The cavity mode is excited with an electric dipole oriented along the dominant mode polarization E_y. This source was set to be a standard Gaussian pulse, centered at the cavity frequency with a narrow bandwidth of 0.88 THz. The total size of the PC structure was $86a \times 75\sqrt{3}a/2$ with the L3 cavity localized at the center of the computational cell. PML boundary conditions and mirror symmetry with respect to the planes $x = 0$, $y = 0$ and $z = 0$ were assumed. Finally, maximum mesh steps of $a/40$ and $0.5\sqrt{3}a/40$ were considered along x and y directions, respectively, while 40 cells per wavelength with a grading factor of 1.41421 were set along the z direction.

Received: 1 February 2021; Accepted: 22 April 2021
Published online: 12 May 2021

References

1. Vahala, K. J. Optical microcavities. *Nature* **424**, 839 (2003).
2. Akahane, Y., Asano, T., Song, B.-S. & Noda, S. High-q photonic nanocavity in a two-dimensional photonic crystal. *Nature* **425**, 944 (2003).
3. Yoshie, T. *et al.* Vacuum rabi splitting with a single quantum dot in a photonic crystal nanocavity. *Nature* **432**, 200 (2004).

4. Englund, D. *et al.* Controlling the spontaneous emission rate of single quantum dots in a two-dimensional photonic crystal. *Phys. Rev. Lett.* **95**, 013904 (2005).
5. Hennessy, K. *et al.* Quantum nature of a strongly coupled single quantum dot-cavity system. *Nature* **445**, 896 (2007).
6. Noda, S., Fujita, M. & Asano, T. Spontaneous-emission control by photonic crystals and nanocavities. *Nat. Photon.* **1**, 449 (2007).
7. Faraon, A. *et al.* Coherent generation of non-classical light on a chip via photon-induced tunnelling and blockade. *Nat. Phys.* **4**, 859 (2008).
8. O'Brien, J. L., Furusawa, A. & Vučković, J. Photonic quantum technologies. *Nat. Photon.* **3**, 687 (2009).
9. Rivoire, K., Lin, Z., Hatami, F., Masselink, W. T. & Vučković, J. Second harmonic generation in gallium phosphide photonic crystal nanocavities with ultralow continuous wave pump power. *Opt. Exp.* **17**, 22609 (2009).
10. Husko, C. *et al.* Ultrafast all-optical modulation in gaas photonic crystal cavities. *Appl. Phys. Lett.* **94**, 021111 (2009).
11. Nomura, M., Kumagai, N., Iwamoto, S., Ota, Y. & Arakawa, Y. Laser oscillation in a strongly coupled single-quantum-dot-nanocavity system. *Nat. Phys.* **6**, 279 (2010).
12. Nozaki, K. *et al.* Sub-femtojoule all-optical switching using a photonic-crystal nanocavity. *Nat. Photon.* **4**, 477 (2010).
13. Galli, M. *et al.* Low-power continuous-wave generation of visible harmonics in silicon photonic crystal nanocavities. *Opt. Exp.* **25**, 26613 (2010).
14. Ellis, B. *et al.* Ultralow-threshold electrically pumped quantum-dot photonic-crystal nanocavity laser. *Nat. Photon.* **5**, 297 (2011).
15. Reinhard, A. *et al.* Strongly correlated photons on a chip. *Nat. Photon.* **6**, 93 (2012).
16. Nozaki, K. *et al.* Ultralow-power all-optical ram based on nanocavities. *Nat. Photon.* **6**, 248 (2012).
17. Volz, T. *et al.* Ultrafast all-optical switching by single photons. *Nat. Photon.* **6**, 605 (2012).
18. Shakoor, A. *et al.* Room temperature all-silicon photonic crystal nanocavity light emitting diode at sub-bandgap wavelengths. *Laser Photon. Rev.* **7**, 114 (2013).
19. Takahashi, Y. *et al.* A micrometre-scale raman silicon laser with a microwatt threshold. *Nature* **498**, 470 (2013).
20. Dharanipathy, U. P., Minkov, M., Tonin, M., Savona, V. & Houdré, R. High-q silicon photonic crystal cavity for enhanced optical nonlinearities. *Appl. Phys. Lett.* **105**, 101101 (2014).
21. Yao, P., Rao, V. M. & Hughes, S. On-chip single photon sources using planar photonic crystals and single quantum dots. *Laser Photon. Rev.* **4**, 499 (2010).
22. Kristensen, P. T. & Hughes, S. Modes and mode volumes of leaky optical cavities and plasmonic nanoresonators. *ACS Photonics* **1**, 2 (2014).
23. Vasco, J. & Hughes, S. Anderson localization in disordered ln photonic crystal slab cavities. *ACS Photon.* **5**, 1262 (2018).
24. Chalcraft, A. R. A. *et al.* Mode structure of the l3 photonic crystal cavity. *Appl. Phys. Lett.* **90**, 241117 (2007).
25. Minkov, M. & Savona, V. Automated optimization of photonic crystal slab cavities. *Sci. Rep.* **4**, 5124 (2014).
26. Tanaka, Y., Asano, T. & Noda, S. Design of photonic crystal nanocavity with q-factor of 10^9. *J. Light. Technol* **26**, 1532 (2008).
27. Minkov, M., Savona, V. & Gerace, D. Photonic crystal slab cavity simultaneously optimized for ultra-high q/v and vertical radiation coupling. *Appl. Phys. Lett.* **111**, 131104 (2017).
28. Asano, T. & Noda, S. Optimization of photonic crystal nanocavities based on deep learning. *Opt. Exp.* **26**, 32704 (2018).
29. Minkov, M., Gerace, D. & Fan, S. Doubly resonant $\chi^{(2)}$ nonlinear photonic crystal cavity based on a bound state in the continuum. *Optica* **6**, 1039 (2019).
30. Wang, J. & Long, Y. On-chip silicon photonic signaling and processing: a review. *Sci. Bull.* **63**, 1267 (2018).
31. Asano, T., Ochi, Y., Takahashi, Y., Kishimoto, K. & Noda, S. Photonic crystal nanocavity with a q factor exceeding eleven million. *Opt. Exp.* **25**, 1769 (2017).
32. Simbula, A. *et al.* Realization of high-q/v photonic crystal cavities defined by an effective aubry-andré-harper bichromatic potential. *APL Photon.* **2**, 056102 (2017).
33. Bazin, A. *et al.* Thermal management in hybrid inp/silicon photonic crystal nanobeam laser. *Opt. Exp.* **22**, 10570 (2014).
34. Borselli, M., Johnson, J. T. & Painter, O. Measuring the role of surface chemistry in silicon microphotonics. *Appl. Phys. Lett.* **88**, 131114 (2006).
35. Lai, Y. *et al.* Genetically designed l3 photonic crystal nanocavities with measured quality factor exceeding one million. *Appl. Phys. Lett.* **104**, 241101 (2014).
36. Asano, T. & Noda, S. Iterative optimization of photonic crystal nanocavity designs by using deep neural networks. *Nanophotonics* **8**, 2243 (2019).
37. Triviño, N. V. *et al.* Gallium nitride l3 photonic crystal cavities with an average quality factor of 16 900 in the near infrared. *Appl. Phys. Lett.* **105**, 231119 (2014).
38. Flayac, H., Minkov, M. & Savona, V. Remote macroscopic entanglement on a photonic crystal architecture. *Phys. Rev. A* **92**, 043812 (2015).
39. Vasco, J., Gerace, D., Seibold, K. & Savona, V. Monolithic silicon-based nanobeam cavities for integrated nonlinear and quantum photonics. *Phys. Rev. Appl* **13**, 034070 (2020).
40. Andreani, L. C. & Gerace, D. Photonic-crystal slabs with a triangular lattice of triangular holes investigated using a guided-mode expansion method. *Phys. Rev. B* **73**, 235114 (2006).
41. Barclay, P. E., Kartik, S. & Painter, O. Nonlinear response of silicon photonic crystal microresonators excited via an integrated waveguide and fiber taper. *Opt. Exp.* **13**, 801 (2005).
42. *Lumerical Solutions, Inc.* https://www.lumerical.com/tcad–products/fdtd/.
43. Song, B.-S., Jeon, S.-W. & Noda, S. Symmetrically glass-clad photonic crystal nanocavities with ultrahigh quality factors. *Opt. Lett.* **36**, 91 (2011).
44. Gerace, D. & Andreani, L. C. Disorder-induced losses in photonic crystal waveguides with line defects. *Opt. Lett.* **29**, 1897 (2004).
45. Minkov, M., Dharanipathy, U. P., Houdré, R. & Savona, V. Statistics of the disorder-induced losses of high-q photonic crystal cavities. *Opt. Exp.* **21**, 28233 (2013).
46. Vasco, J. & Savona, V. Disorder effects on the coupling strength of coupled photonic crystal slab cavities. *New J. Phys.* **20**, 075002 (2018).
47. Mohamed, M. S. *et al.* Influence of disorder and finite-size effects on slow light transport in extended photonic crystal coupled-cavity waveguides. *ACS Photon.* **5**, 4846 (2018).
48. Dodane, D., Bourderionnet, J., Combrié, S. & de Rossi, A. Fully embedded photonic crystal cavity with q=0.6 million fabricated within a full-process cmos multiproject wafer. *Opt. Express* **26**, 20868 (2018).

Author contributions

J.P. Vasco and V. Savona equally contributed to the simulation and analysis of all results, as well as the preparation of the manuscript.

Competing interests

The authors declare no competing interests.

Additional information

Supplementary information The online version contains supplementary material available at https://doi.org/10.1038/s41598-021-89410-1.

Correspondence and requests for materials should be addressed to J.P.V.

Reprints and permissions information is available at www.nature.com/reprints.

Publisher's note Springer Nature remains neutral with regard to jurisdictional claims in published maps and institutional affiliations.

Open Access This article is licensed under a Creative Commons Attribution 4.0 International License, which permits use, sharing, adaptation, distribution and reproduction in any medium or format, as long as you give appropriate credit to the original author(s) and the source, provide a link to the Creative Commons licence, and indicate if changes were made. The images or other third party material in this article are included in the article's Creative Commons licence, unless indicated otherwise in a credit line to the material. If material is not included in the article's Creative Commons licence and your intended use is not permitted by statutory regulation or exceeds the permitted use, you will need to obtain permission directly from the copyright holder. To view a copy of this licence, visit http://creativecommons.org/licenses/by/4.0/.

© The Author(s) 2021